J Sol-Gel Sci Technol (2016) 77:416–422
DOI 10.1007/s10971-015-3869-z

ORIGINAL PAPER

Sol–gel synthesis of nanoparticles of gamma alumina and their application in defluoridation of water

I. B. Singh[1] · Akanksha Gupta[2] · Swati Dubey[1] · M. Shafeeq[1] · P. Banerjee[1] · A. S. K. Sinha[2]

Received: 18 June 2015 / Accepted: 16 September 2015 / Published online: 1 October 2015

Abstract Water solvent-based sol–gel process was employed in the synthesis of nanoparticles of gamma alumina (NPGA) which were used for the removal of fluoride from water of neutral pH. Different techniques like thermogravimetric analysis, Fourier transform infrared spectroscopy, X-ray diffraction, and field emission scanning electron microscopy were employed for the characterization of the synthesized particles. Batch adsorption studies were performed for the optimization of contact time and adsorbent doses to obtain maximum fluoride removal and understanding of the adsorption kinetics and mechanism. The maximum adsorption capacity of NPGA for fluoride removal was estimated to be nearly 14 mg/g at room temperature (30 °C) which is better than fluoride removal reported by earlier using of commercial-grade NPGA. Adsorption kinetics measurement indicated that Langmuir equilibrium model is found to be more suitable for describing the fluoride adsorption mechanism.

Graphical Abstract

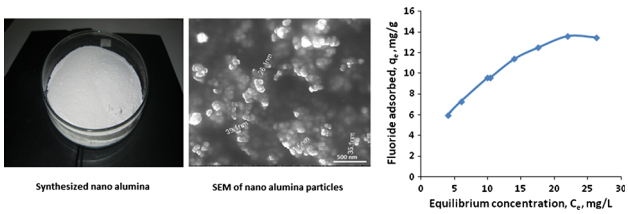

✉ I. B. Singh
ibsingh58@yahoo.com

[1] CSIR-Advanced Materials and Process Research Institute, Bhopal 462026, MP, India

[2] Department of Chemical Engineering, Indian Institute of Technology, Banaras Hindu University, Varanasi 221005, UP, India

Keywords Gamma alumina · Nanoparticles · Adsorption kinetics · Defluoridation of water

1 Introduction

Fluoride contamination of water due to the natural (e.g., geochemical reactions and volcanic emissions) and anthropogenic activities (e.g., mining and industrial chemical wastes) is a major problem all over the world [1]. In addition, discharge of the fluoride-bearing wastewater from drugs, cosmetics, semiconductor, glass and ceramic production, electroplating, and rubber and fertilizer manufacturing industries also increases fluoride contamination of groundwater [2, 3]. Fluoride is an essential element for building healthy teeth and inhibiting dental carries of human beings. As per World Health Organization (WHO), the optimum fluoride level in drinking water should lie below 1.5 mg/l [4]. Consumption of excess fluoride-bearing drinking water causes dental caries, skeletal fluorosis, cancer, and damages of brain and kidney [5]. It is estimated that around 70 million people or even more are suffering from fluorosis problem across the world. In India, 19 states are affected by various form of fluorosis problem [6].

Several methods like ion exchange, precipitation, reverse osmosis, adsorption, electrodialysis, and membrane filtration have been applied to reduce excessive fluoride of water [7–13]. Among them, adsorption is an ideal and appropriate method because of its simplicity and availability of a variety of adsorbents. Activated alumina is known as the most effective adsorbent for reducing fluoride level in drinking water [14–16]. It can be prepared by different methods from aluminum salts. Among their various phases known, gamma alumina (γ-Al_2O_3) is considered the most effective adsorbent because of its high

surface area, enhanced reactivity for adsorption, mass transfer efficiency, etc. [17–19]. Adsorption capacity of nanoscale metal oxide particles with a very high surface-to-volume ratio enhances sorption capacity further more as compared to their microcrystalline surfaces because the sorption or binding sites reside maximum on the surface [20–22]. However, only a few reports are available in the literature dealing with the applications of nanoscale metal oxides especially nanoalumina particles for the removal of fluoride and other anions from water [18–22].

There are several methods like mechanical milling, vapor phase reaction at high temperature, combustion method, sol–gel method, and precipitation method are being used in the synthesis of nanoceramic particles. Among them, sol–gel process has attracted a considerable amount of interest in the preparation of ceramics nanoparticles [23–27]. In this process, morphology, homogeneity, and surface area of the particles can be easily controlled. Sol–gel synthesis of alumina particles comprises hydrolysis of aluminum alkoxide in water to obtain boehmite (AlOOH) as gel and its calcination at 400–800 °C to produce γ-Al_2O_3 after releasing one molecule of water as per following reaction (1)

$$2\mathrm{AlOOH} \rightarrow \mathrm{Al_2O_3} + \mathrm{H_2O} \quad (1)$$

Hydrolysis of alkoxide is generally carried out either in aqueous (water) or non-aqueous (alcohol) solvent. Use of water as solvent is cost-effective, and hydrolysis reaction can be made in open system. In the present work, boehmite gel was prepared using water as solvent followed by their calcination at 500 °C to produce nanoparticles of gamma alumina (NPGA). The synthesized NPGA derived from sol–gel synthesis through aqueous system has been used for the first time, for the adsorption of fluoride of water in this present study.

2 Experimental procedure

All chemicals used in the synthesis of boehmite gel and fluoride analysis were of reagent grades. Based on Yoldas process [28], boehmite gel was synthesized using aluminum isopropoxide and double-distilled water in their 1:100 molar ratio. Details of synthesis of boehmite are available elsewhere [29, 30]. After drying, it was calcined in muffle furnace for 1 h at 500 °C. Finally, the calcined substrate was grounded using mechanically operated agate mortar pistil.

Thermogravimetric and differential thermal analysis (TGA/DSC) were performed in a Mettler Toledo analyzer (SF/1100). The samples were analyzed under an inert atmosphere of nitrogen up to 900° C. TGA/DSC profiles were obtained by plotting the relative weight (%) of the sample against temperature. To study the functional groups and bond characteristics of the synthesized alumina particles, Fourier transform infrared spectroscopy (FTIR) was employed using FTIR (Model Nicolet 5700) in the range 4000–400 cm^{-1}. Surface area of the synthesized particles was analyzed by BET (Brunauer, Emmett and Teller), using Micromeritics-made ASAP 2020 model. X-ray diffraction (XRD) analysis was used for the confirmation of gamma phase of the synthesized particles using Rigaku Miniflex 2 model. Field emission scanning electron microscope (FEI-made FESEM Nova NanoSEM 430 model) was used in the examination of morphology of the synthesized particles.

Adsorption kinetics was carried out at room temperature (30 ± 2 °C) using batch experiment. Stock solution of 1000 mg/l fluoride solution was prepared by dissolving 2.211 g of sodium fluoride (NaF) in 1 l distilled water. Working solutions of 10 mg/l fluoride was made by successive dilution of the stock solution. Thereafter, adsorption studies were performed in 150-ml borosil-made conical flask by taking different quantity of adsorbent in 100 ml fluoride-bearing working solution. pH of the working solution was kept at 7 by adjusting with dilute sodium hydroxide (NaOH) and hydrochloric acid (HCl). Conical flasks containing working solution were kept on rotary shaker at 80 rpm for different durations. After analysis of residual fluoride, adsorption capacity of the nanoparticles was derived as per relation

$$q_e = \int_0^{VE} (C_0 - C)\, \mathrm{d}V/m \quad (2)$$

where q_e is the fluoride adsorbed (mg/g), C_0 is the total fluoride concentration (mg/l) of the working solution, C is the residual fluoride concentration (mg/l) left after batch adsorption, VE is the volume of solution, and m is the mass of the adsorbent used in the batch process.

Residual fluoride was analyzed using alizarin red visual method [31, 32]. Alizarin red indicator was prepared by making two sets of solution. The first set of solution was prepared by dissolving 300 mg zirconyl chloride octahydrate ($ZrOCl_2$) and 71 mg alizarin red dye (3-alizarin sulfonic acid sodium salt) in 500 ml distilled water. The second set of solution was prepared by taking 101 ml concentrated HCL and 33 ml concentrated H_2SO_4 in 500 ml water. Both solutions were mixed in 1-l volumetric flask. After mixing, solution became red in color mainly due to the formation of complex ions of zirconium and dye. In the presence of fluoride ions, zirconium ions get replaced by fluoride ion from the complexes resulting in reappearance of original yellow color of zirconium. Concentration of residual fluoride was determined by comparing color of standard solution of fluoride in water. The intensity of yellow color depends on the concentration of

residual fluoride present in the working solution. In preparation of standard solution, blank (0.0), 0.2, 0.4, 0.6, 0.8, 1.0, and 1.2 mg/l fluoride-bearing water solutions were prepared in 50-ml-volume nessler tube. Five milliliters of prepared alizarin red indicator was added in each solution which showed different shades of color from dark red (blank) to faded yellow (fluoride bearing). Solutions were also prepared from the filtrates obtained after batch adsorption in identical condition. Analysis results obtained by alizarin visual method were cross checked by spectrophotometer (Hack39000) using SPANDS solution [31].

3 Results and discussion

3.1 Characterization of the synthesized particles

Figure 1 shows the TGA and DSC curves of synthesized boehmite. TGA curve shows 5–6 % weight loss in the temperature range of 50–150 °C. Occurrence of an endothermic peak at 75–100 °C in the DSC curve suggests weight loss due to the elimination of physically adsorbed water. Another endothermic peak in the temperature range of 400–480 °C with significant weight loss (15–20 %) in the TGA curve is associated with dehydration of boehmite in alumina formation. The weight loss in the 400–500 °C range in the TGA is mainly due to the removal of water molecule during transformation of boehmite to alumina. According to Guzman-Castillo et al. [33] and Rinaldi and Schuchardt [34], the transition from boehmite to gamma Al_2O_3 takes place between 380 and 580 °C temperature range. Based on this, present TGA/DSC analysis confirms the formation of gamma alumina after calcinations of boehmite at 500 °C.

XRD diffractograms obtained for the calcined boehmite at 500 °C is shown in Fig. 2. The obtained diffractograms

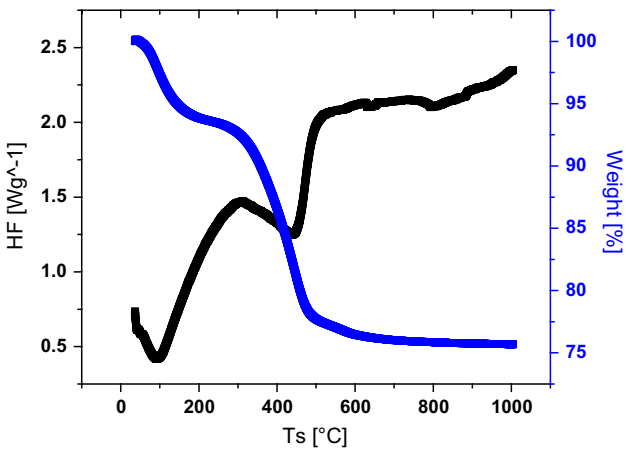

Fig. 1 TGA/DSC of sol–gel synthesized boehmite

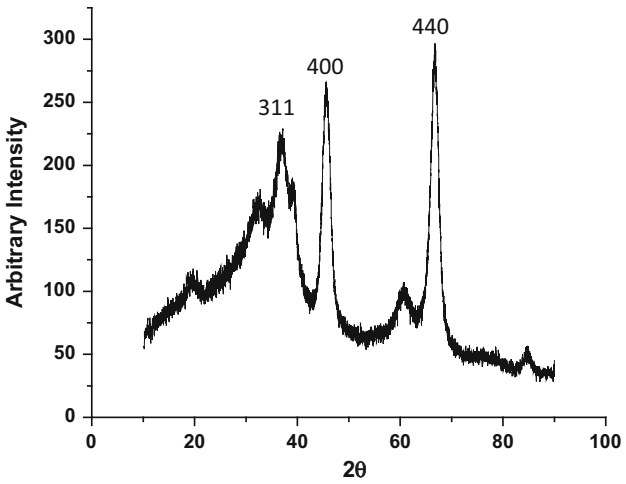

Fig. 2 FTIR of sol–gel synthesized boehmite sintered at 500 °C

are matching well with XRD standard for gamma alumina structure (JCPDS reference no. 00-010-0425). XRD pattern shows three distinct reflections at 37.2° (311 reflection), 45.805° (400), and 66.779° (440) which is in agreement with the database standard and also the powder XRD studies of Lippens [35]. We calculated the crystallite size using the Debye–Scherrer equation from the width of the XRD peak. The crystalline sizes derived from the (400) and (440) reflections occur as 31.8 and 25.3 nm, respectively. This shows the average crystallite size of the synthesized particle would be in the range around 30 nm. XRD analysis indicates that the boehmite convert to gamma alumina after calcinations at 500 °C, the well-known process for the preparation of fine gamma alumina from boehmite [36, 37].

Formation of gamma alumina was further confirmed by measuring FTIR spectrum (Fig. 3). Gamma alumina is known to have a spinel structure which exists over a range of hydrogen content captured by the empirical formula $H_{3m}Al_{2-m}O_3$ [38]. IR spectra as shown in Fig. 3 explain the existence of bond-stretching vibration corresponding to –OH bond and Al–O–Al bond at different frequencies. Occurrence of a strong broadening band between 3800 and 3000 cm^{-1} is due to stretching vibration of −OH in hydration water. Another stronger broadening band between 900 and 5000 cm^{-1} corresponds to Al–O–Al vibration [39]. Existence of Al–O–Al vibration confirms the presence of alumina.

The morphology of the synthesized particles was determined by FESEM analysis. The image of the synthesized particles is as depicted in Fig. 4, showing particles in agglomerated form. The size of the particle determined by scale bar seems to be 30 nm as average size. The surface area of the particle determined by BET analysis was found to be 137 m^2/g. Synthesis process was repeated thrice, and we observed a reproducible characterization values as discussed above.

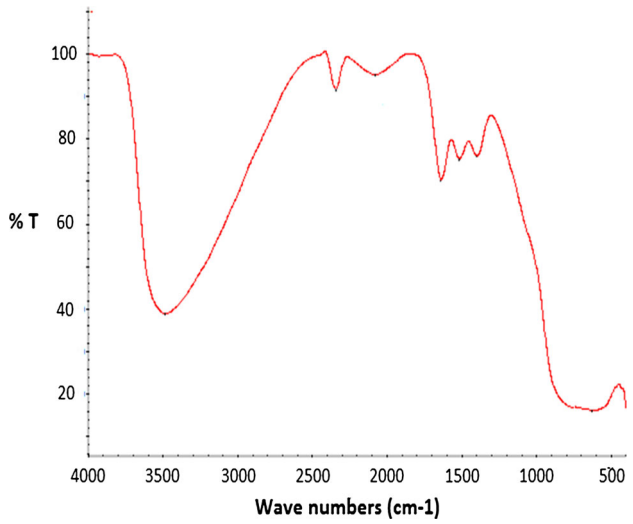

Fig. 3 XRD of sol–gel synthesized boehmite sintered at 500 °C

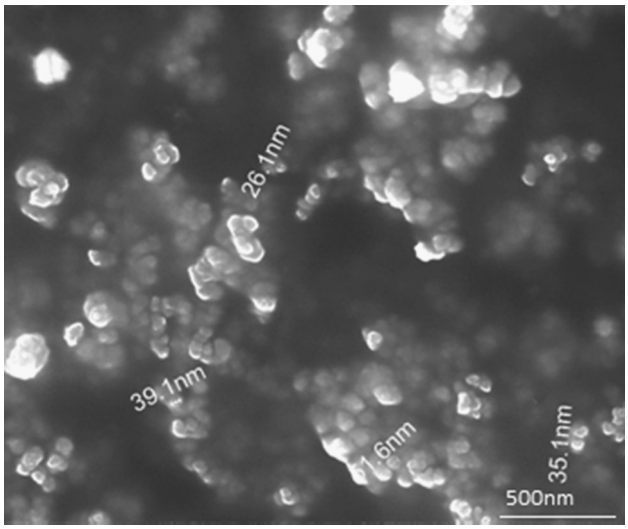

Fig. 4 SEM image of synthesised nanoparticles of gamma alumina

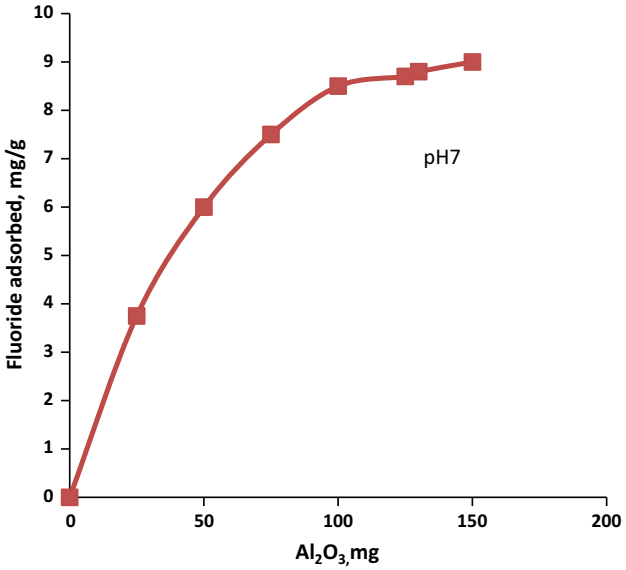

Fig. 5 Effect of adsorbent doses on the fluoride removal

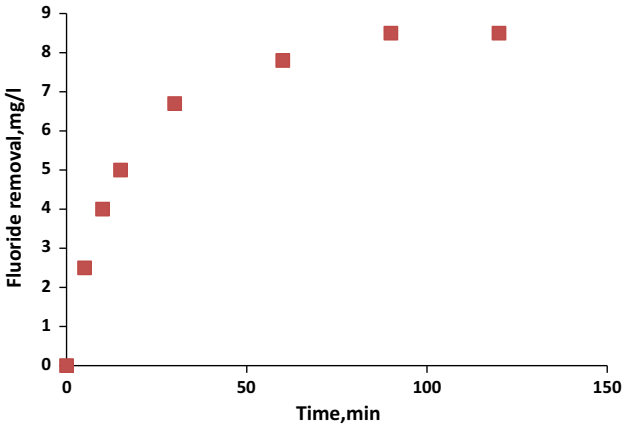

Fig. 6 Effect of contact time on the fluoride removal

3.2 Fluoride adsorption kinetic

The effect of pH on the adsorption of alumina is studied well [19, 22]. It is generally observed that fluoride removal occurs maximum in the pH 5–7 of water as electrostatic attraction of negatively charged fluoride ion and positively charged adsorbent are mostly available in this pH range. Since water of pH 7 is more practical for drinking purposes, we carried out fluoride removal study at this pH. In this study, 25, 50, 75, 100, 125, and 150 mg synthesized nanoparticles were mixed in 10 mg/l fluoride containing 100 ml water solution in conical flask. Afterward, conical flasks were mechanically shaken for 90 min. Figure 5 shows fluoride removal trend in the presence of different doses of synthesized particles. It can be seen that maximum fluoride removal occurs as 9 mg/g in the presence of 125 mg of the nanoalumina. After this, increase in dose did not make any noticeable improvement in fluoride removal. Fluoride removal trend determined after taking 100 mg doses depicts two different stages of fluoride adsorption (Fig. 6). Initially, fluoride adsorption occurs with fast rate as 60 % fluoride ions and get adsorbed within 30 min of contact time. After this, the adsorption reaction slows down as it takes another 50 min to get maximum (85 %) adsorption of fluoride ions. Occurrence of a fast rate of fluoride adsorption in the initial stage is mainly due to the availability of sufficient sites at the adsorbent. With passage of time, the availability of the vacant sites in the adsorbent reduces. This results in increase in contact time as remaining (un-adsorbed) fluoride ions have to cover more distance to reach the vacant sites of the adsorbent.

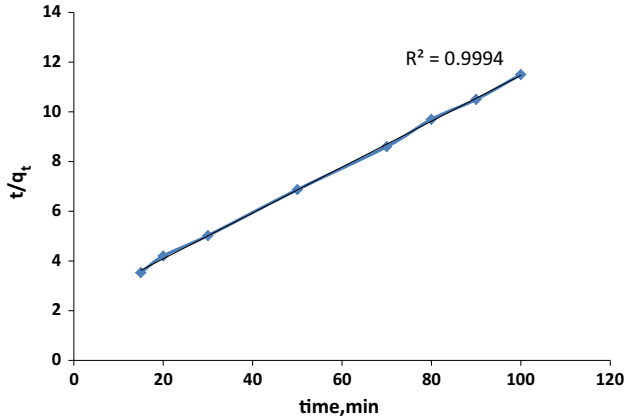

Fig. 7 Pseudo-second-order kinetic plots of fluoride sorption on nanoparticles of gamma alumina

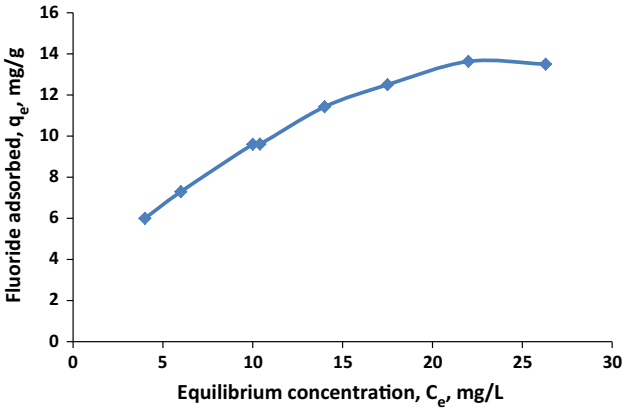

Fig. 8 Adsorption isotherm of fluoride on synthesized nanoparticles of gamma alumina (contact time 90 min, adsorbent doses 100 mg)

Observed trend is similar to those reported previously for fluoride adsorption on the nano particles of gamma alumina [19, 22].

The pseudo-second-order kinetics is reported to occur in the adsorption of fluoride ions at nanoparticles of alumina or activated alumina [14, 19, 40]. We verified this by utilizing pseudo-second-order model as per following Eq. (3)

$$t/q_t = (1/k_s q_e^2) + (1/q_e)t \quad (3)$$

After analyzing data as presented in Fig. 7, we found best-fit pseudo-second-order reaction kinetics as linear correlation coefficient (R^2) occurs as 0.9994 which is very close to unity. To estimate maximum adsorption capacity of the synthesized nanoparticle, the equilibrium of fluoride adsorption was studied by plotting q_e versus C_e (Fig. 8). It can be noticed that nearly 14 mg/g adsorption occurs after reaching of saturation state. Present trends indicate that adsorption capacity increases gradually with an increase in equilibrium fluoride concentration. Gradual rise in the isotherm suggests the availability of accessible sites for adsorption during the initial phase. Saturation of adsorption sites attains at the plateau where fluoride adsorption occurs as 13.85 mg/g. In fluoride adsorption, simple electrostatic replacement reaction of OH^- and F^- is involved with the Al^{3+} of alumina [40]. Langmuir and Freundlich isotherms were analyzed as per given Eqs. 4 and 5, respectively

$$1/q_e = 1/q_m + 1/bC_e q_m \quad (4)$$

$$\log(q_e) = \log(k_f) + \log(C_e) + 1/n \quad (5)$$

where q_e is the amount of fluoride adsorbed at equilibrium concentration C_e, q_m is a Langmuir constant which represents maximum monolayer adsorption capacity, b is Langmuir constant related to activation energy, k_f and $1/n$ are Freundlich constants associated with adsorption capacity and adsorption intensity, respectively. Freundlich isotherm is based on the assumption that the adsorbing

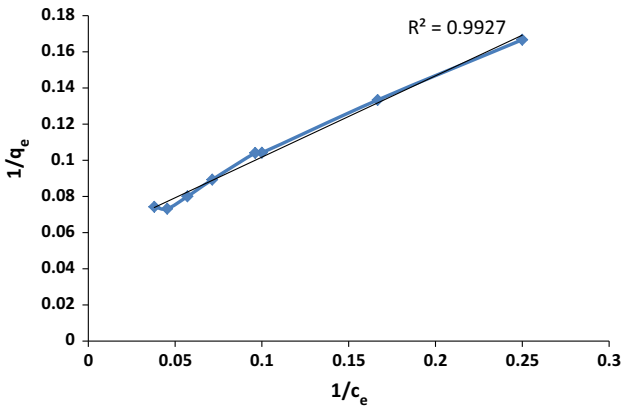

Fig. 9 Langmuir adsorption isotherm of fluoride adsorption on the on synthesised nanoparticles of gamma alumina

surface is energetically heterogeneous, consisting of adsorption sites of differing energies, whereas Langmuir isotherm based on the assumption that all adsorption active sites are homogeneous and that the ability of a molecule to interact with a site on the surface of the adsorbent is independent of whether neighboring sites are occupied or not. In addition, adsorption is restricted to a monolayer without lateral interactions between adsorbed molecules. Figures 9 and 10 represent Langmuir and Freundlich isotherm models, respectively. The correlation coefficient (R^2) is derived as 0.993 for Langmuir and 0.974 for Freundlich isotherm. Langmuir isotherm model fits the data best as it shows better correlation coefficient as compared to Freundlich isotherm. In Langmuir model, the adsorption process follows the formation of a monolayer of fluoride adsorbate on the surface of the synthesized NPGA. Different values derived from Freundlich and Langmuir sorption models are given in Table 1. From the obtained data, it can be seen that the value of q_m occurs as 13.44 mg/g which is near to the maximum value (13.85 mg/g)

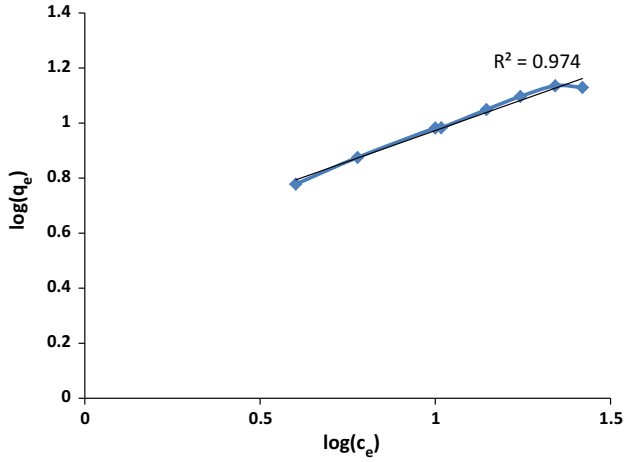

Fig. 10 Freundlich adsorption isotherm of fluoride adsorption on synthesized nanoparticles of gamma alumina

Table 1 Langmuir and Freundlich isotherm parameters obtained for the adsorption of fluoride ion on synthesized gamma nanoalumina particles

Langmuir isotherm		Freundlich isotherm	
q_m (mg/g)	13.44	$1/n$	0.444
b (l/mg)	0.132	k_f (mg/g)	1.68
R^2	0.993	R^2	0.974

observed at the saturation state (Fig. 8). Kumar et al. [19] measured an increased rate of fluoride adsorption on NPGA with an increase in pH, reaching maximum at pH 6.15 and then decreasing with further increment in the pH. In the present case, we observed as 13.85 mg/g fluoride removal. Kumar et al. [19] obtained 14 mg/g fluoride adsorption at pH 6.15 on commercial-grade NPGA, a Sigma-Aldrich product. However, their fluoride removal rate could have been much lower at pH 7 because they observed a steep reduction on adsorption rate from 50 % (at pH 6.15) to 20 % at pH 7–9. If this is the case, then present synthesized NPGA exhibit excellent potential of fluoride adsorption even at neutral pH.

Fluoride adsorption at the alumina surfaces in aqueous medium is the result of replacement of adsorbed hydroxyl ions by fluoride ions. According to Hu et al. [41], fluoride and hydroxide ions form $Al_nFm(OH)_{3n-m}$ complexes with Al(III) ions as per following reaction,

$$n\mathrm{Al}^{3+}_{(aq)} + 3n - m\mathrm{OH}^{-}_{(aq)} + m\mathrm{F}^{-}_{(aq)} \rightarrow \mathrm{Al}_n\mathrm{F}_m(\mathrm{OH})_{3n-m(s)} \quad (6)$$

On the basis of spectroscopic analysis, Zhang et al. [42] described that fluoride ions enter the surface of alumina by substituting hydroxyl group without breaking the bridging Al–O–Al bond. Based on this, the mechanism of fluoride adsorption can be described by following two-step reaction,

$$n\mathrm{Al}^{3+} + 3n - m\mathrm{OH}^{-} \rightarrow \mathrm{Al}_n(\mathrm{OH})_{3n-m}(\text{adsorption reaction}) \quad (7)$$

$$\mathrm{Al}_n(\mathrm{OH})_{3n-m} + 3n - m\mathrm{F}^{-} \rightarrow \mathrm{Al}_n(\mathrm{F})_{3n-m} + 3n - m\mathrm{OH}^{-}(\text{substitution reaction}) \quad (8)$$

In the first step, electrostatic interaction between positively charged alumina and negatively charged hydroxide ions make $Al_n(OH)_{3n-m}$ at the alumina surfaces. In the presence of fluoride ions, $Al_n(F)_{3n-m}$ forms after substitution of hydroxyl ions. Since fluoride ion possesses greater affinity with Al^{3+}, it makes a competitive role in the replacement of the hydroxyl ions.

4 Conclusions

Present sol–gel synthesis process utilizing water as solvent appears to be simple and feasible method for preparation of NPGA in large scale. Different characterization studies confirm the formation of pure and crystallite particles of gamma alumina of around 30 nm of average size. Fluoride removal study indicates that synthesized nanoparticles show better fluoride removal potential as compared to fluoride removal reported on commercial-grade NPGA. Fluoride adsorption kinetics follows pseudo-second-order kinetics. The adsorption isotherm is fitted well with Langmuir model describing the occurrence of single-layer adsorption at the synthesized nanoparticles surface. A maximum adsorption capacity derived from the adsorption isotherms occurs nearly 14 mg/g in water of neutral pH.

Acknowledgments Authors would like to thank Director, CSIR-AMPRI, for providing experimental facilities and also his approval to one of the author (AG) to carry out her internship without any financial assistance.

References

1. Das DP, Parida K (2003) Physicochemical characterization and adsorption behavior of calcined Zn/Al hydrotalcite-like compound (HTlc) towards removal of fluoride from aqueous solution. J Colloid Interface Sci 261:213–220
2. Raichur AM, Basu MJ (2001) Adsorption of fluoride onto mixed rare earth oxides. Sep Purif Technol 24:121–127
3. Shen F, Chen X, Gao P, Chen G (2003) Electrochemical removal of fluoride ions from industrial wastewater. Chem Eng Sci 58:987–993
4. World Health Organization (WHO) (2004) Guidelines for drinking-water quality, 3rd edn. WHO, Geneva
5. Latham MC (1997) Human nutrition in the developing world. Food and Agriculture Organisation, United Rome

6. Susheela AK (2002) Fluorisis in developing countries: remedial measures and approaches. Proc Indian Natl Sci Acad B68: 389–400
7. Saha S (1993) Treatment of aqueous effluent for fluoride removal. Water Res 27:1347–1350
8. Amor Z, Mameri BN, Taky M, Nicolas S, Elmidaoui A (2001) Fluoride removal from brackish water by electrodialysis. Desalination 133:215–223
9. Ghorai S, Pant KK (2004) Investigations on the column performance of fluoride adsorption by activated alumina in a fixed-bed. Chem Eng 981:65–173
10. Ndiaye PI, Moulin P, Dominguez L, Millet JC, Charbit F (2005) Removal of fluoride from electronic industrial effluent by RO membrane separation. Desalination 173:25–32
11. Singh IB, Prasad M (2004) Study on fluoride removal characteristic of mineral (fluorapatite). Ind J Chem Technol 11:185–189
12. Singh IB, Prasad M, Amritphale S (2004) Development of defluridation technology for its easy adaptation in rural areas. J Rural Technol 1:163–166
13. Daifullah AAM, Yakout SM, Elreefy SA (2007) Adsorption of fluoride in aqueous solutions using $KMnO_4$-modified activated carbon derived from steam pyrolysis of rice straw. J Hazard Mater 147:633–643
14. Leyva-Ramos R, Medellin-Castillo NA, Jacobo-Azuara A, Landin Mendoza-Barron J, Rodriguez LE, Martinez-Rosales JM, Aragon-Piña A (2008) Fluoride removal from water solution by adsorption on activated alumina prepared from pseudo-boehmite. J Environ Eng Manage 18:301–309
15. Fawel J, Bailey K, Chilton J, Dahi E, Fewtrell L, Magara Y (2006) Fluoride in drinking-water. IWA Publishing, London
16. Onyango MS, Matsuda H (2006) Fluoride removal from water using adsorption technique. In: Tressaud A (ed) Fluorine and the environment. Elsevier, B V, Amsterdam, pp 1–48
17. Jovancic P, Radetic M, Barcelo D, Petrovic M (eds) (2008) Emerging contaminants from industrial and municipal waste: removal technologies (The handbook of environmental chemistry/water pollution), vol 5. Springer, Berlin, Heidelberg, pp 239–264
18. Hristovski K, Baumgardner A, Westerhoff P (2007) Selecting metal oxide nano materials for arsenic removal in fixed bed columns: from nanopowders to aggregated nanoparticle media. J Hazard Mater 147:265–274
19. Kumar E, Bhatnagar A, Kumar U, Sillanp M (2011) Defluoridation from aqueous solution by nano alumina: characterization and sorption studies. J Hazard Mater 186:1042–1049
20. Puttamraju P, SenGupta AK (2006) Evidence of tunable on–off sorption behaviors of metal oxide nanoparticles: role of ion exchanger support. Ind Eng Chem Res 45:7737–7742
21. Zhao X, Shi Y, Cai Y, Mou S (2008) Cetyltrimethylammonium bromide-coated magnetic nanoparticles for the preconcentration of phenolic compounds from environmental water samples. Environ Sci Technol 42:1201–1206
22. Zhao X, Wang J, Wu F, Wang T, Cai Y, Shi Y, Jiang G (2010) Removal of fluoride from aqueous media by Fe_3O_4 & $Al(OH)_3$ magnetic nanoparticles. J Hazard Mater 173:102–109
23. Wu M, Lin G, Chen D, Wang G, He D, Feng S, Xu R (2002) Sol hydrothermal synthesis and hydrothermally structural evolution of nano crystalline titanium dioxide. Chem Mater 14:1974–1980
24. Yanagisawa K, Rendon-Angeles JC, Kanai H, Yamashita Y (2000) Stability and single crystal growth of lead scandium niobate and its solid-solution with lead titanate under hydrothermal conditions. J Mater Sci 35:3011–3015
25. Yang Q, Li Y, Yin Q, Wang P, Cheng Y-B (2002) Hydrothermal synthesis of bismuth oxide needles. Mater Lett 55:46–49
26. Rozman M, Drofenik M (1995) Hydrothermal synthesis of manganese zinc ferrite. J Am Ceram Soc 78:2449
27. Wang CC, Ying JY (1999) Sol–gel synthesis and hydrothermal processing of anatase and rutile titania nanocrystals. Chem Mater 11:3113–3120
28. Yoldas BE (1975) Alumina sol preparation from alkoxides. Am Ceram Soc Bull 51:289–290
29. Singh IB, Ruhi G, Modi OP (2015) Development of sol–gel alumina coating on 9Cr–1Mo steel and their oxidation behavior at high temperature. J Sol-Gel Sci Technol 74:685–691
30. Ruhi G, Modi OP, Singh IB (2009) Effect of sintering atmosphere on the corrosion and wear resistance of sol–gel alumina coated mild steel surface. Corrosion 65:758–764
31. Greenberg AE (ed) (1985) Standard methods for the examination of water and waste water. American Public Health Association (APHA), Washington DC
32. Chena N, Zhang Z, Fenga C, Lia M, Sugiurab N (2011) Investigations on the batch and fixed-bed column performance of fluoride adsorption by Kanuma mud. Desalination 268:76–82
33. Guzman-Castillo ML, Hernandez-Beltran F, Fripiat JJ, Rodriguez- Hernandez A, Garcia de Leon R, Navarrete-Bolanos J, Tobon-Cervantes A, Bokhimi X (2005) Physicochemical properties of aluminas obtained from different aluminum salts. Catal Today 107–108:874–878
34. Rinaldi R, Schuchardt U (2005) On the paradox of transition metal-free alumina catalyzed oxidation with aqueous hydrogen peroxide. J Catal 236:335–345
35. Lippens BC, Boer JH (1964) Study of phase transformations during calcinations of Al hydroxides by selected electron diffraction. Acta Crystallogr 17:1312
36. Liu Q, Guo H, Shan Y (2010) Adsorption of fluoride on synthetic siderite from aqueous solution. J Fluor Chem 131:635–641
37. Misra C (1986) Industrial alumina chemicals, ACS Monograph184. American Chemical Society, Washington DC
38. Sohlberg K, Pennycook SJ, Pantelides ST (1999) Hydrogen and the structure of the transition aluminas. J Am Ceram Soc 121:7493
39. Frederickson LD (1954) Characterization of hydrated aluminas by infrared spectroscopy: application to study of bauxite ores. Anal Chem 26:1883–1885
40. Ho YS, McKay G (1999) Pseudo-second-order model for sorption processes. Biochem 34:451–465
41. Hu CY, Lo SL, Kuan WH (2005) Effects of the molar ratio of hydroxide and fluoride to Al(III) on fluoride removal by coagulation and electro-coagulation. J Colloid Interface Sci 283: 472–476
42. Zhang W, Sun M, Prins R (2002) Multinuclear MAS NMR identification of fluorine species on the surface of fluorinated γ-alumina. J Phys Chem B 106:11805–11809